Sucrose phosphorylase from Alteromonas mediterranea : structural insight into the regioselective α-glucosylation of (+)-catechin

Marine Goux, Marie Demonceaux, Johann Hendrickx, Claude Solleux, Emilie Lormeau, Folmer Fredslund, David Tezé, Bernard Offmann, Corinne André-Miral

Sucrose phosphorylase from *Alteromonas mediterranea*: structural insight into the regioselective α-glucosylation of (+)-catechin

Marine Goux[a,c], Marie Demonceaux[a,d], Johann Hendrickx[a,e], Claude Solleux[a], Emilie Lormeau[a], Folmer Fredslund[b,f], David Tezé[b,g], Bernard Offmann[a,h,j] and Corinne André-Miral[a,i,j]

[a] Nantes Université, CNRS, US2B, UMR 6286, F-44000, Nantes, France

[b] DTU Biosustain, Technical University of Denmark, DK-2800 Kgs. Lyngby, Denmark

[c] ORCID number: 0000-0002-8350-4102, e-mail : marine.goux-huet@univ-nantes.fr

[d] ORCID number: 0000-0002-6090-4007, e-mail : marie.demonceaux@univ-nantes.fr

[e] ORCID number: 0000-0002-3988-2747, e-mail : johann.hendrickx@univ-nantes.fr

[f] ORCID number: 0000-0003-0881-1927, e-mail : folf@biosustain.dtu.dk

[g] ORCID number: 0000-0002-6865-6108, e-mail : datez@biosustain.dtu.dk

[h] ORCID number: 0000-0002-6845-5883, e-mail : bernard.offmann@univ-nantes.fr

[i] ORCID number: 0000-0002-3378-2331, e-mail : corinne.miral@univ-nantes.fr

[j] Corresponding authors: Corinne André-Miral and Bernard Offmann

Abstract

Flavonoids glycosylation at different positions is paramount to solubility and modulation of bioactivities. Sucrose phosphorylases, through transglycosylation reactions, are interesting enzymes that can transfer glucose from sucrose, the donor substrate, onto polyphenols to form glycoconjugates. Here, we report for the first time the structural and enzymatic properties of sucrose phosphorylase from the marine bacteria *Alteromonas mediterranea* (*Am*SP). We characterized and investigated the transglucosylation capacity of two new variants of the enzyme on (+)-catechin and their propensity to catalyse its regioselective glucosylation. *Am*SP-Q353F and

*Am*SP-P140D were shown to catalyse the regiospecific glucosylation of (+)-catechin using sucrose as donor substrate. While AmSP-WT was devoid of synthetic activity, each of its two single mutant provided high yields of specific regioisomers: 89% of (+)-catechin-4′-O-α-D-glucopyranoside (CAT-4') for AmSP-P140D and 92% of (+)-catechin-3′-O-α-D-glucopyranoside (CAT-3') for AmSP-Q353F. The novel compound CAT-4' was fully characterized by NMR and mass spectrometry. We used molecular docking simulations on structural models of the glucosyl-enzyme intermediate to explain this regioselectivity. We showed that *Am*SP-P140D preferentially binds (+)-catechin in a mode that favours glucosylation on its hydroxyl group in position 4' (OH-4') while the binding mode of the flavonoid in AmSP-Q353F favoured glucosylation on its hydroxyl group in position 3' (OH-3').

Keywords: marine microbial enzymes, regioselectivity, biocatalysis, (+)-catechin, sucrose-phosphorylase, *Alteromonas mediterranea*

1. Introduction

Oceans cover more than 70% of Earth's surface and provides a unique environment to marine bacteria (*i.e.* high salinity, high pressure, low temperature and special lighting conditions). For decades, enzymes have been isolated and purified from terrestrial microorganisms, animals and plants. With the advent of biotechnology, there has been a growing interest and demand for enzymes with novel properties and robust biocatalysts. Due to its complexity, the marine environment represents a great opportunity for exploration of new enzymes and molecules [1, 2]. Marine enzymes are capable of being active under extreme conditions, which provide competitiveness and efficiency to different industrial processes [3, 4]. Among those, sucrose-phosphorylases (SPs) from the Glycoside Hydrolase family 13 subfamily 18 (GH13_18, EC 2.4.1.7) attract biotechnological interest as biocatalysts. Requiring only a cheap and abundant donor, SPs can perform transglucosylation reaction by transferring glucose from sucrose to an acceptor to

yield α-glucosylated products with a retaining mechanism *via* a β-glucosyl-enzyme intermediate. Particularly, *Bifidobacterium adolescentis* SP (*Ba*SP-WT) and its mutants have been studied for biocatalytic synthesis of rare disaccharides [5, 6] and α-glucosylation of polyphenols [7, 8, 9, 10]. To date, the only documented structures of sucrose phosphorylase in the literature are from *Bifidobacterium adolescentis* [11]. Other SPs, from *Leuconostoc mesenteroides*, *Streptococcus mutans*, *Lactobacillus acidophilus* and *Thermoanaerobacterium thermosaccharolyticum*, have also been studied for the glucosylation of phenolic compounds [12, 13, 14]. Glucosylation of this type of molecules increases their solubility in water and their bioavailability in health, nutraceuticals and cosmetics applications [15, 16]. Controlling the regioselectivity of this glucosylation is also at stake for the synthesis of new compounds. We recently documented the activity of two variants of *Ba*SP-WT with respect to their ability to transfer regioselectively a glucose moiety onto (+)-catechin as an acceptor substrate [10]. *Ba*SP-Q345F and *Ba*SP-P134D/Q345F glucosylated (+)-catechin on hydroxyl groups in position 3' (OH-3') and 5 (OH-5) with obtainment of three glucosylated regioisomers: (+)-catechin-3′-O-α-D-glucopyranoside (CAT-3'), (+)-catechin-5-O-α-D-glucopyranoside (CAT-5) and (+)-catechin-3',5-O-α-D-diglucopyranoside (CAT-3',5), with a ratio of 51:25:24 for *Ba*SP-Q345F and 82:9:9 for *Ba*SP-P134D/Q345F.

Alteromonas mediterranea, also known as *Alteromonas macleodii* "Deep Ecotype" or AltDE, is an aerobic Gram-negative and mesophilic marine bacterium from the genus of *Proteobacteria* which was first isolated at a depth of 1000 m in the Eastern Mediterranean Sea in 2005 [17, 18, 19]. Wild type form of *Am*SP (*Am*SP-WT) shares 52% of global sequence identity with *Ba*SP-WT. Sequence alignments revealed that both enzymes possess highly conserved regions corresponding to the loop A (*Ba*SP-WT: ^{336}AAASNLDLYQ^{345}, *Am*SP-WT: ^{344}AAASNLDLYQ^{353}) and loop B (*Ba*SP-WT: ^{132}YRPRP^{136}, *Am*SP-WT: ^{138}FRPRP^{142}) of the catalytic site [20]. In a preliminary screening using homology modelling and molecular docking, we identified that the catalytic cavity of the glucosyl-intermediate of *Am*SP-WT could potentially host a polyphenolic acceptor compound like (+)-

catechin. We thus characterized *Am*SP-WT from a structural and functional perspective. Towards this end, the crystallographic structure of *Am*SP-WT was for the first time recently determined [Goux *et al.*, in preparation]. In the present work, we further analysed the structural features of *Am*SP-WT and investigated the enzymatic properties of two variants of the enzyme towards their propensity to catalyse the regioselective transglucosylation of (+)-catechin. P140D and Q353F mutations, homologous to mutations P134D and Q345F of *Ba*SP-WT, displayed a single transfer reaction product for each enzyme: (+)-catechin-4′-O-α-D-glucopyranoside (CAT-4') for *Am*SP-P140D and CAT-3' for *Am*SP-Q353F. To explain the striking enzymatic activities of those variants, we provide in-depth structural insights by docking simulations and modelling. Our results interestingly broaden the available chemo-enzymatic synthetic tools for the efficient regioselective α-glucosylation of polyphenols.

2. Materials and methods

2.1. Vector construction and proteins

*Am*SP-WT and its variants were expressed as C-terminally hexahistidine-tagged proteins, allowing affinity purification by standard protocols. *Am*SP-WT gene (UniProt: S5AE64_9ALTE) was ordered from Genscript already cloned in a pET28b vector. E. coli BL21(DE3) competent cells (Novagen) were transformed with pET28b_*Am*SP-WT. Clones were selected using LB-agar medium supplemented with 25 µg/mL kanamycin and confirmed by Sanger sequencing (Eurofins Genomics). Variants *Am*SP-P140D, *Am*SP-Q353F and *Am*SP-P140D/Q353F were obtained by site-directed mutagenesis. Proteins were produced, purified and characterized as previously described [10].

2.2. *Transglucosylation studies*

Reactions were carried out in 50 mM 3-morpholinopropane-1-sulfonic acid (MOPS)-NaOH solution at pH 8.0 in a total volume of 1 mL. Reaction mixture containing 10 mM (+)-catechin in DMSO (1 eq., 100 µL), 10% DMSO (100 µL, (v/v)), 80 mM sucrose in H_2O (8 eq., 100 µL) was incubated with a final concentration of 10 µM of purified enzyme at 25°C under slight agitation. Enzymatic synthesis was monitored by thin layer chromatography (TLC) for 48h. TLC plates were developed in solution composed of ethyl acetate/methanol/cyclohexane/water (6.75:1.35:1:0.9, v/v/v/v) with 0.1% formic acid (v/v). Products were visualized using a UV lamp at 254 nm and revealed with vanillin-sulphuric acid reagent.

2.3. *Purification and analysis of glucosylated (+)-catechin*

After centrifugation (12 000 x *g*, 20 min), 10 µL of the supernatant was analysed by analytical HPLC at 280 nm on a C-18 column (Interchim, 5 µm, 250 x 4.6 mm, US5C18HQ-250/046) with an isocratic flow of 80% H_2O (v/v), 0.1% formic acid (v/v) and 20% MeOH (v/v), 0.1% formic acid (v/v) for 20 min. Then, remaining supernatant was purified by HPLC at 280 nm on a C-18 column (Interchim, 5 µm, 250 x 21.2 mm, US5C18HQ-250/212) with a gradient system (solvent A: H_2O HCOOH 0.1%; solvent B: MeOH, HCOOH 0.1%; t0 min = 70/30, t10 min = 70/30, t70 min = 10/90). Products were identified by NMR ^{1}H and ^{13}C in MeOD or DMSO-d_6 (400 Hz, 256 scans). For characterization of CAT-3', CAT-5 and CAT-3',5, see [10].

2.4. *Molecular modelling of variants of AmSP-WT*

Glucosyl-enzyme intermediate 3D-models were built for *Am*SP-Q353F and *Am*SP-P140D using the following procedure and the Rosetta software [22]. Glucosylated-aspartyl 192 residue from chain A of crystal structure of *Ba*SP-WT (PDB: 2GDV-A) was inserted into the crystal structure *Am*SP-WT

(PDB: 7ZNP) that served as initial template for both variants. As this glucosylated aspartyl is a non-standard residue, it was absent from the database of the Rosetta software. Using Pymol3, the initial coordinates of this modified residue were retrieved. While this residue (D192) and the glucose moiety (BGC) are covalently linked in the crystal structure, the Pymol software considered them as two distinct residues. Thus, they were merged them into a single non-standard residue, which was called with a new ID, DGC. Associated charges and rotamers were calculated for this new residue using the Rosetta software. All those data were merged a single file that we added into the Rosetta database (Section 2.7).

With the DGC residue ready to be used, glucosyl-intermediates were built for the two variants of *Am*SP-WT. From the crystal structure (PDB: 7ZNP), using Rosetta the native aspartyl residue in position 203 was mutated by the glucosylated-aspartyl DGC residue together with either the P140D or Q353F mutation. For each variant (*Am*SP-Q353F or *Am*SP-P140D), a sample of 50 conformers was generated thanks to the program Backrub from Rosetta suite, with 10 000 tries. In parallel, 12 conformers of (+)-catechin were also generated using the Mercury software (CCDC) [23] from the crystal structure OZIDOR of (+)-catechin.

2.5. Docking analysis of binding mode of (+)-catechin in the catalytic pocket

All docking experiments were performed with AutoDock Vina using the glucosyl-intermediates and (+)-catechin conformers built above. Docking perimeter was limited to the residues of the active site of the enzyme. Each of the 12 conformers of (+)-catechin were docked on every conformer of the two variants. This amounts to a total of 600 (50x12) docking experiments for each variant of the enzyme. Only the productive poses that could lead to a glucosylation of (+)-catechin were selected. To do so, docking poses were filtered using the following distance constraints: distances within 3.0 Å between any oxygen of (+)-catechin and the anomeric carbon atom C1 of the glucosyl moiety were assessed. Docking scores were compiled for these productive poses and compared

between the two variants. R statistics software package was used to perform the boxplots analysis.

3. Results

3.1. Highly conserved structural features and potential activity of AmSP-WT

Through structural comparison of *Ba*SP-WT (PDB: 1R7A, 2GDV), *Ba*SP-Q345F (PDB: 5C8B), and our recently determined structure of *Am*SP-WT (PDB: 7ZNP), we identified the conserved residues likely involved in the reaction mechanism and potential substrate interactions (Table S1). The −1 subsite of SPs, also called donor site, has an optimal topology for binding glucose and is conserved between *Ba*SP-WT and *Am*SP-WT (Figure 1). The configuration of the two catalytic residues involved in the reaction mechanism are also almost identical (Figure 1A, in blue): a glutamyl residue acts as a general acid/base catalyst (E243 for *Am*SP-WT and E232 for *Ba*SP-WT) and an aspartyl residue performs the nucleophilic attack (D203 for *Am*SP-WT and D192 for *Ba*SP-WT). The third member of the catalytic triad (D301 for *Am*SP-WT and D290 for *Ba*SP-WT) stabilises the transition state with a strong hydrogen bond and presents also an identical configuration in the catalytic site. The structural elements that were shown to stabilize the glucosyl moiety in *Ba*SP-WT by non-polar contacts between a hydrophobic platform (F53/F156 for *Ba*SP-WT) and the hydrophobic C3-C4-C5 part of glucose are also conserved in *Am*SP-WT (F56/F167). The acceptor or +1 site of SPs is mainly shaped by two highly dynamic loops (Figure S1), which were shown to adopt different conformations based on the progress of the reaction mechanism: one conformation is the “donor binding mode” or closed conformation and the other is the “acceptor binding mode” or open conformation where an arginyl residue (R135 in *Ba*SP-WT) is thought to enable the enzyme to outcompete water as an acceptor through strong electrostatic interactions. When we compare the apoenzyme of *Ba*SP-WT (PDB: 1R7A) with our newly obtained apoenzyme

of *Am*SP-WT (PDB: 7ZNP), a striking difference in the positioning of loop A is noticed. The enzyme has already an opened conformation and is in the "acceptor binding mode" with Y352 residue pointing inside the active site (Figure 1, in magenta) and R141 pointing outside (Figure 1, in orange). This open conformation was also observed for *Ba*SP-WT crystallized with the end-product of the reaction after hydrolysis of glucose (PDB: 2GDV, chain B). Moreover, crucial conserved residues involved in binding of both phosphate and fructose, Y196 and H234 for *Ba*SP-WT *vs.* Y207 and H245 for *Am*SP-WT, are in the same conformational positions thus allowing sucrose phosphorylase activity (Figure 1B, in cyan)[21]. In *Ba*SP-WT, Y132 is located at the entrance of the active site and contributes to sucrose specificity thanks to hydrophobic interactions with Y196 and F206. In *Am*SP-WT, the aromatic structure is conserved with the replacement of the tyrosinyl moiety by a phenylalanyl residue in position 138 (Figure 1B, in orange).

3.2. Determination of the apparent kinetic parameters

Interestingly, the P140D and Q353F mutations did not alter the enzyme stability, as evidenced by unchanged melting temperature (T_m) of 43°C (Figure S2, Table S2). The apparent kinetic parameters for sucrose at 25°C with and without 20% DMSO were determined. For each condition, variants present a decrease of catalytic efficiency towards sucrose of one order of magnitude compared to the wild-type (Table 1). A loss in specificity for sucrose was observed for *Am*SP-Q353F with an increasing of the K_m value from 1 mM for *Am*SP-WT to 5 mM for *Am*SP-Q353F. With DMSO, *Am*SP-P140D displayed a higher specificity for sucrose with a K_m value similar to the wild-type, resulting in a catalytic efficiency increasing by almost 2-fold compared to the results obtained without DMSO. For *Am*SP-Q353F, with 20% of DMSO, we observed no change for the specificity for sucrose and the turnover number.

3.3. (+)-catechin transglucosylation studies

We assessed the ability of SPs to transfer a glucose moiety from sucrose to (+)-catechin at 25°C after 24h under agitation. Observed products were purified by preparative HPLC and analysed by NMR. *Am*SP-P140D and *Am*SP-Q353F, catalyse efficiently the synthesis of two different regioisomers of (+)-catechin glucoside: *Am*SP-P140D glucosylate mostly the hydroxyl groups in position 4' (OH-4') while *Am*SP-Q353F glucosylate the OH-3' position (Figure S5, Table S4). We monitored the synthesis of glucosylated (+)-catechin products during 24h by HPLC to determine conversion yields and proportion of regioisomers (Figure 2, Table 2). Interestingly, the main product formed with *Am*SP-P140D was CAT-4' with a relative proportion of 89% while the main product formed with AmSP-Q353F was CAT-3' with a relative proportion of 92%. The corresponding synthetic yields (percentage of (+)-catechin that was converted into these glycosylated products) was 26% and 82% respectively. These results clearly indicate that these two variants are highly regioselective with respect to their transglycosylation activities on (+)-catechin.

3.4. Structural insights into the regioselectivity of AmSP-P140D and AmSP-Q353F

To further understand the observed regioselectivities, we performed molecular docking simulations with several conformations of the glucosyl intermediate of *Am*SP-Q353F and *Am*SP-P140D. The preferred orientations of various (+)-catechin conformers in the acceptor site of the glucosyl-enzyme intermediate were assessed using docking protocols implemented in Autodock Vina. Docking poses were filtered for reactivity, by considering those with an oxygen of (+)-catechin within 3 Å of the C1 atom of the glucosyl moiety as productive. Docking results were consistent with the observed experimental regioselectivity. For *Am*SP-Q353F, productive poses for glucosylation of (+)-catechin in OH3' position is overwhelmingly favoured energetically when

compared to the other hydroxyl groups (OH-4', OH-5 and in position 7) of the flavonoid (Figure S6). On the other hand, for *Am*SP-P140D, the most favoured productive poses for glucosylation of (+)-catechin is on OH-4' position (Figures S6). Comparison of the binding energies of the productive poses of (+)-catechin towards OH-3' and OH-4' glucosylation provided in Figure 3A clearly explains the observed regioselectivity. For each enzyme, structural analysis of the best productive poses showed a distance of 3.0 Å between the C1 atom of the glucosyl moiety and the OH-3' or OH-4' of (+)-catechin, and a distance with D203 residue of 4.0 Å (Figure 3B and 3C). For *Am*SP-P140D, (+)-catechin is stabilized in the active +1 site by a network of 4 hydrogen bonds and numerous hydrophobic contacts (Figure 4).

4. Discussion

In glycochemistry, the fine control of the regioselectivity is the Holy Grail in enzymatic reactions catalysed by glycosyl hydrolase (GHs) such as sucrose phosphorylase. A disadvantage of GHs is their moderate regioselectivity, meaning that a mixture of products is often formed when the acceptor contains more than one hydroxyl group. Previously, for (+)-catechin which consists of five phenolic hydroxyl groups, we generated with *Ba*SP-Q345F and *Ba*SP-P134D/Q345F a mixture of glucosylated regioisomers: CAT-3', CAT-5 and CAT-3',5 with a ratio of 51:25:24 for *Ba*SP-Q345F and 82:9:9 for *Ba*SP- P134D/Q345F. Another drawback is the relatively low product yields. With the same variants, we obtained a synthetic yield of 34%/15%/9% and 40%/5%/4%, respectively. In the active site of the SPs, the −1 site is rigid to allow a high selectivity on glucose while the +1 site is more flexible and can accept several types of acceptors or leaving groups. The +1 site of *Am*SP-WT, is mainly shaped by two highly labile loops, loop A (^{344}AAASNLDLYQ^{353}) and loop B (^{138}FRPRP^{142}), which undergo crucial conformational changes throughout the catalytic cycle suited for binding either fructose or phosphate. Crystal structure of *Am*SP-WT shows a wide access channel capable of accommodating naturally large polyphenolic acceptors. By site-directed mutagenesis, we

substituted the residue Q353 in loop B into F353 and/or the residue P140 into D140 in Loop A. We obtained three variants: *Am*SP-P140D, *Am*SP-Q353F and *Am*SP-P140D/Q353F. The double variant showed no improvement for the synthesis of CAT-3' with the obtainment of a mixture of products at 25°C (data not shown). By engineering the residue 353 of the active site, we enhanced the enzyme regioselectivity from a mixture of products to OH-3' position almost exclusively. Docking studies confirmed that the most favoured pose for (+)-catechin in the catalytic +1 site of *Am*SP-Q353F lead to the formation of CAT-3'. As seen with *Ba*SP-Q345F, we hypothesized that the introduction of F353 as a potential partner for π–π stacking leads to rearrangements in loop A with a shift of Y352 which can stabilise (+)-catechin in the active site by hydrophobic interactions. *Ba*SP-Q345F, *Ba*SP-P134D/Q345F and *Am*SP-Q353F preferentially glucosylate the OH-3' position of flavonoids while ignoring the OH-4' position. This was confirmed by docking simulations which highlighted that the most favoured pose for (+)-catechin in the catalytic site of AmSP-Q353F (Figure 3 and Table 2) would lead to the regioselective formation of CAT-3'. Surprisingly, while BaSP-P140D was not active, *Am*SP-P140D leads to the regioselective formation of CAT-4' (Figure 3 and Table 2). Thus, switching Q353F mutation to P140D had shift completely the regioselectivity of *Am*SP-WT from CAT-3' to CAT-4'. An explanation enlightened by molecular modelling is the steric hindrance caused by F138/Y207/F217 residues between *Am*SP-P140D and the polyphenol rings (Figures 3B and S7). Indeed, we observed that the conformation of the acceptor site drastically changed and seems to allow only an almost linear orientation of all three (+)-catechin rings. Contrarily to *Am*SP-Q353F, those very strong constraints lead to the regioselective glucosylation of the OH-4' position of the flavonoid with a high proportion (89%).

5. Conclusion

In this study, we provided the first report of the use of variants of sucrose phosphorylase from *Alteromonas mediterranea* for the regioselective transglucosylation of (+)-catechin and the

synthesis of a novel compound fully characterized, (+)-catechin-4′-O-α-D-glucopyranoside (CAT-4'). *Am*SP-Q353F and *Am*SP-P140D are able to synthesize regioselectively compound CAT-3' and CAT-4', with a proportion of 92% and 89%, respectively. With *Am*SP-P140D, we succeed to switch the regioselectivity from OH-3' to OH-4'-glucosylated (+)-catechin. Mutation P140D changes drastically the conformation of the acceptor site and seems to allow an almost linear alignment of the glucose moiety and of all three (+)-catechin rings allowing selectively the glucosylation of the position OH-4' of this flavonoid. Overall, the results described herein suggest that *Am*SP-Q353F and *Am*SP-P140D are suitable for the enzymatic regioselective synthesis of polyphenolic glucosides at high yields and could facilitate the synthesis of *de novo* products in OH-4' position using other phenolic phytochemicals such as quercetin or kaempferol.

Supporting information

For details about melting curves, kinetic parameters analysis, HPLC/MS, NMR spectra, etc., please see provided Electronic Supplementary Information.

Author Contributions

MG and MD wrote the original draft. MG, MD, CM, BO and JH developed the methodology. MG, MD, CS and EL performed the experimental investigation and the following analysis. DT and FF obtained the crystallographic structure of *Am*SP-WT. JH and BO performed the molecular and docking simulations and the following analysis. CM obtained the funding, designed and directed the project. All authors discussed the results and contributed to the final manuscript.

Conflicts of interest

There are no conflicts to declare.

Acknowledgments

MG post-doctoral fellowship was supported by the “Region Pays de la Loire” and “Université Bretagne Loire” within the project “FunRégiOx”, and MD thesis by “Nantes Université”. We thank the CEISAM NMR platform for the NMR experiments.

References

[1] A. Beygmoradi, A. Homaei, R. Hemmati, Marine chitinolytic enzymes, a biotechnological treasure hidden in the ocean?, Appl. Microbiol. Biotechnol. 102 (2018) 9937–9948. https://doi.org/10.1007/s00253-018-9385-7

[2] V.S. Bernan, M. Greenstein, M.W. Maiese, Marine microorganisms as a source of new natural products, Adv. Appl. Microbiol. 43 (1997) 57-90. https://doi.org/10.1016/s0065-2164(08)70223-5.

[3] H. Harmsen, D. Prieur, C. Jeanthon, Distribution of microorganisms in deep-sea hydrothermal vent chimneys investigated by whole-cell hybridization and enrichment culture of thermophilic subpopulations, Appl. Environ. Microbiol. 63 (1997) 2876-2883. https://doi.org/10.1128/aem.63.7.2876-2883.1997.

[4] T.H. Cheng, N. Ismail, N. Kamaruding, Industrial enzymes-producing marine bacteria from marine resources, Biotechnology Reports. 27 (2020) e00482. https://doi.org/10.1016/j.btre.2020.e00482.

[5] M. Kraus, J. Görl, M. Timm, Synthesis of the rare disaccharide nigerose by structure-based design of a phosphorylase mutant with altered regioselectivity, ChemComm 52 (2016) 4625–4627. https://doi.org/10.1039/c6cc00934d.

[6] J. Franceus et al., “Rational design of an improved transglucosylase for production of the rare sugar nigerose, ChemComm. 55 (2019) 4531–4533. https://doi.org/10.1039/c9cc01587f.

[7] M. Kraus, C. Grimm, J. Seibel, Redesign of the Active Site of Sucrose Phosphorylase through a Clash-Induced Cascade of Loop Shifts, ChemBioChem 17 (2016) 33–36. https://doi.org/10.1002/cbic.201500514.

[8] M. Kraus, C. Grimm, J. Seibel, “Switching enzyme specificity from phosphate to resveratrol glucosylation, ChemComm. 53 (2017) 12181–12184. https://doi.org/10.1039/c7cc05993k.

[9] D. Aerts, T. F. Verhaeghe, B. I. Roman, Transglucosylation potential of six sucrose phosphorylases toward different classes of acceptors, Carbohydr. Res. 346 (2011) 1860-1867. https://doi.org/10.1016/j.carres.2011.06.024.

[10] M. Demonceaux, M. Goux, M., J. Hendrickx, Regioselective glucosylation of (+)-catechin using a new variant of the sucrose phosphorylase from *Bifidobacterium adolescentis*, Org. Biomol. Chem. 11 (2023). https://doi.org/10.1039/d3ob00191a.

[11] D. Sprogoe, L.A.M. van den Broek, O. Mirza, Crystal structure of sucrose phosphorylase from Bifidobacterium adolescentis, Biochemistry 43 (2004) 1156-1162. https://doi.org/10.1021/bi0356395.

[12] M. E. Dirks-Hofmeister, T. Verhaeghe, K. De Winter, Creating Space for Large Acceptors: Rational Biocatalyst Design for Resveratrol Glycosylation in an Aqueous System, Angew. Chemie. 54 (2015) 9289–9292. https://doi.org/10.1002/anie.201503605.

[13] S. Kitao, T. Ariga, T. Matsudo, The Syntheses of Catechin-glucosides by Transglycosylation with Leuconostoc Mesenteroides Sucrose Phosphorylase, Biosci. Biotechnol. Biochem. 57 (1993). 2010–2015, 1993, https://doi.org/10.1271/bbb.57.2010.

[14] K. De Winter, G. Dewitte, M.E. Dirks-Hofmeister, Enzymatic Glycosylation of Phenolic Antioxidants: Phosphorylase-Mediated Synthesis and Characterization, Journal of

Agricultural and Food Chemistry 2015 63 (46) 10131-10139. https://doi.org/10.1021/acs.jafc.5b04380

[15] K. De Winter, A. Cerdobbel, W. Operational stability of immobilized sucrose phosphorylase: continuous production of α-glucose-1-phosphate at elevated temperatures. Process Biochem. 46 (2011) 1074–1078. https://doi.org/10.1016/j.procbio.2011.08.002.

[16] J. Franceus, T. Desmet, Sucrose Phosphorylase and Related Enzymes in Glycoside Hydrolase Family 13: Discovery, Application and Engineering, Int. J. Mol. Sci. 21 (2020) 2526. https://doi.org/10.3390/ijms21072526

[17] A. López-López, S.G. Bartual, L. Stal, Genetic analysis of housekeeping genes reveals a deep-sea ecotype of Alteromonas macleodii in the Mediterranean Sea, Environ Microbiol. 7 (2005)649-659. https://doi.org/10.1111/j.1462-2920.2005.00733.x

[18] E.P. Ivanova, M. López-Pérez, M. Zabalos, Ecophysiological diversity of a novel member of the genus Alteromonas, and description of Alteromonas mediterranea sp. nov. Antonie Van Leeuwenhoek. 107 (2015) 119-132. https://doi.org/10.1007/s10482-014-0309-y

[19] M. López-Pérez, A. Gonzaga, A.B. Martin-Cuadrado, Genomes of surface isolates of Alteromonas macleodii: the life of a widespread marine opportunistic copiotroph. Sci Rep 2, 696 (2012). https://doi.org/10.1038/srep00696

[20] O. Mirza, L.K. Skov, D. Sprogoe, Structural Rearrangements of Sucrose Phosphorylase from Bifidobacterium adolescentis during Sucrose Conversion, J. Biol. Chem. 281 (2006) 35576-35584. https://doi.org/10.1074/jbc.M605611200.

[21] T. Verhaeghe, M. Diricks, D., Mapping the acceptor site of sucrose phosphorylase from Bifidobacterium adolescentis by alanine scanning, J. Mol. Catal 96 (2013) 81-88. https://doi.org/10.1016/j.molcatb.2013.06.014

[22] C. A. Rohl, C.E. Strauss, K.M. Misura, Protein structure prediction using Rosetta, Methods Enzymol. 383 (2004) 66–93. https://doi.org/10.1016/S0076-6879(04)83004-0

[23] R. Schumacker and S. Tomek, Understanding Statistics Using R, Springer, 2013. https://doi.org/10.1007/978-1-4614-6227-9

[24] R. A. Laskowski, M. B. Swindells, LigPlot+: multiple ligand-protein interaction diagrams for drug discovery. J. Chem. Inf. Model., 51 (2011) 2778-2786. https://doi.org/10.1021/ci200227u

Figures caption and legend

Figure 1: Crystallographic structures of *Ba*SP-WT and *Am*SP-WT focused on residues involved in (A) sucrose and (B) fructose binding. (A) In magenta: Loop A (in sticks for *Ba*SP-WT: Y344/D342, in sticks for *Am*SP-WT: Y352/D350); orange: Loop B (in sticks for *Ba*SP-WT: R135, in sticks for *Am*SP-WT: R141); and blue: residues of the catalytic triad (in sticks for *Ba*SP-WT: D192/E232/D290, in sticks for *Am*SP-WT: D203/E243/D301). **(B)** In magenta: Loop A (in sticks for *Ba*SP-WT: D342/L343/Y344/Q345, in sticks for *Am*SP-WT: D350/L351/Y352/Q353); orange: Loop B (in sticks for *Ba*SP-WT: Y132/R133/P134/R135, in sticks for *Am*SP-WT: F138/R139/P140/R141); Cyan: residues involved in sucrose phosphorylase activity (in sticks for *Ba*SP-WT: Y196/V233/H234, in sticks for *Am*SP-WT: Y207/I244/H245).

Figure 2: Products profile of *Am*SP-Q353F and *Am*SP-P140D using (+)-catechin as acceptor. Proportion of each regioisomers was calculated from the area under the curves obtained by analytical HPLC (isocratic mode at 80% H_2O (v/v), 0.1% formic acid (v/v) and 20% MeOH (v/v), 0.1% formic acid (v/v)).

Figure 3: Structural rearrangement of *Am*SP active site and best productive poses of (+)-catechin towards OH-3' and OH-4' for *Am*SP-P140D (B) and *Am*SP-Q353F (C) glucosyl-enzyme. (A) Comparison of binding energy of productive poses of (+)-catechin towards OH-3' and OH-4' for *Am*SP-P140D and *Am*SP-Q353F glucosyl-enzyme (ΔG = -9.3 kcal/mol for *Am*SP-Q353F and -9.2 kcal/mol for *Am*SP-P140D). In magenta: Loop A with in sticks Y352/D350/Q(F)353 residues; orange: Loop B with in sticks R141/F138 and D140 for *Am*SP-P140D; blue: residues of the catalytic triad with in sticks D203/D301/DGC243; and pink : (+)-catechin.

380 **Figure 4. Analysis of the interaction between (+)-catechin and AmSP-P140D.** Shown are hydrogen
381 bonds and hydrophobic contacts between the (+)-catechin substrate (denoted Kxn1) and the
382 interacting residues including the glucosylated-aspartyl (Dgc203). The diagram was obtained using
383 LigPlot Plus v.2.2 [24].
384

Table 1: Apparent kinetic parameters for sucrose hydrolysis by AmSP and its variants. Reactions were conducted in MOPS 50 mM pH 8.0 at 25°C with or without 20% of DMSO. Values are based on Michaelis-Menten fittings obtained with Microsoft Excel. Hanes-Woolf plots are included in the electronic supplementary information (Figures S3 and S4).

	0% DMSO			**20% DMSO**		
	K_M **(mM)**	k_{cat} **(s^{-1})**	k_{cat}/K_M	K_M **(mM)**	k_{cat} **(s^{-1})**	k_{cat}/K_M
***Am*SP-WT**	0.8 ± 0.2	120 ± 34	156.6 ± 26.2	0.91 ± 0.1	109 ± 12	124.6 ± 7.6
***Am*SP-P140D**	1.8 ± 0.5	13 ± 2.0	7.34 ± 1.4	1.02 ± 0.4	19 ± 4.0	20.12 ± 7.1
***Am*SP-Q353F**	4.6 ± 1.2	2 ± 0.0	0.46 ± 0.1	4.23 ± 0.8	3 ± 0.0	0.79 ± 0.1

Table 2: Synthetic yields (A) and relative proportion (B) of (+)-catechin glycosylated products obtained with P140D and Q353F variants of AmSP. Synthetic yields are expressed as a percentage of (+)-catechin that was converted into the corresponding glycosylated products (CAT-4': (+)-catechin-4′-O-α-D-glucopyranoside; CAT-3': (+)-catechin-3′-O-α-D-glucopyranoside; CAT-5: (+)-catechin-5-O-α-D-glucopyranoside; CAT3',5: (+)-catechin-3',5-O-α-D-diglucopyranoside). The relative proportion of each product was calculated from the area under the curves obtained by analytical HPLC at 24 h with the same conditions than for Figure S5.

	Synthetic yields				**Proportion of each product**			
Product	**CAT-4'**	**CAT-3'**	**CAT-5**	**CAT-3',5**	**CAT-4'**	**CAT-3'**	**CAT-5**	**CAT-3',5**
P140D	26.36%	3.21%	Traces	Traces	89.08%	10.92%	Traces	Traces
Q353F	3.49%	82.64%	2.22%	1.85%	3.93%	91.58%	2.28%	2.21%

Electronic Supplementary Information

Sucrose phosphorylase from *Alteromonas mediterranea*: structural insight into the regioselective α-glucosylation of (+)-catechin

Marine Goux[a,c], Marie Demonceaux[a,d], Johann Hendrickx[a,e], Claude Solleux[a], Emilie Lormeau[a], Folmer Fredslund [b], David Tezé [b], Bernard Offmann[a,f,h] and Corinne André-Miral[a,g,h]

[a] Nantes Université, CNRS, US2B, UMR 6286, F-44000, Nantes, France

[b] DTU Biosustain, Technical University of Denmark, DK-2800 Kgs. Lyngby, Denmark

[c] ORCID number: 0000-0002-8350-4102, e-mail : marine.goux-huet@univ-nantes.fr

[d] ORCID number: 0000-0002-6090-4007, e-mail : marie.demonceaux@univ-nantes.fr

[e] ORCID number: 0000-0002-3988-2747, e-mail : johann.hendrickx@univ-nantes.fr

[f] ORCID number: 0000-0002-6845-5883, e-mail : bernard.offmann@univ-nantes.fr

[g] ORCID number: 0000-0002-3378-2331, e-mail : corinne.miral@univ-nantes.fr

[h] Corresponding authors: Corinne André-Miral and Bernard Offmann

Table of Contents

Sucrose phosphorylase from *Alteromonas mediterranea*: structural insight into the regioselective α-glucosylation of (+)-catechin 1

Characteristics of *Am*SP and its variants 3

Sequence of AmSP-WT including His-tag on C-term 3

Structural homology between BaSP and AmSP 4

Determination of the apparent kinetic parameters 8

(+)-catechin transglycosylation studies 10

Synthesis yields 10

^{1}H and ^{13}C NMR Spectral Data of CAT-4' in DMSO 12

Characteristics of *Am*SP and its variants

Sequence of AmSP-WT including His-tag on C-term

```
  1 MGSIRNGVQL ITYADRLGDG NIESLTNLLD GPLKGLFKGV HILPFYYPYD GEDAGFDPID
 61 HTTVDERLGD WNNIKKLGES VDIMADLIVN HMSGQSEAFT DVLKKGRESE YWPLFLTKED
121 VFSGNDQAEI DEQIAKVFRP RPTPFFSDYE VGIETDSTET VPFWTTFTSN QIDIDVESEL
181 GKEYLSSILQ SFTESNVDLI RLDAAGYAIK RAGSNCFMLE ETFEFIEALS KRARTMGMQC
241 LVEIHSHYQT QIDIAARCDS VYDFALPPLV LHTLFTKDAS ALAHWLSISP RNCFTVLDTH
301 DGIGIVDVGA SGDKPGLISA DAINALVEQI HVNSNGESKK ATGAAANNVD LYQVNCTYYD
361 ALGKDDFAYL VARAIQFFSP GIPQVYYGGL LAAHNDMELL ANTNVGRDIN RPYLTTAMVE
421 DAIQKPVVKG LMQLITLRNE NKAFGGAFDV TYTDNTLVLS WSNDGDAASL TVDFAAMDAT
481 INTVSNGEES TLSIGALLAH HHHHH
```

Structural homology between BaSP and AmSP

A.

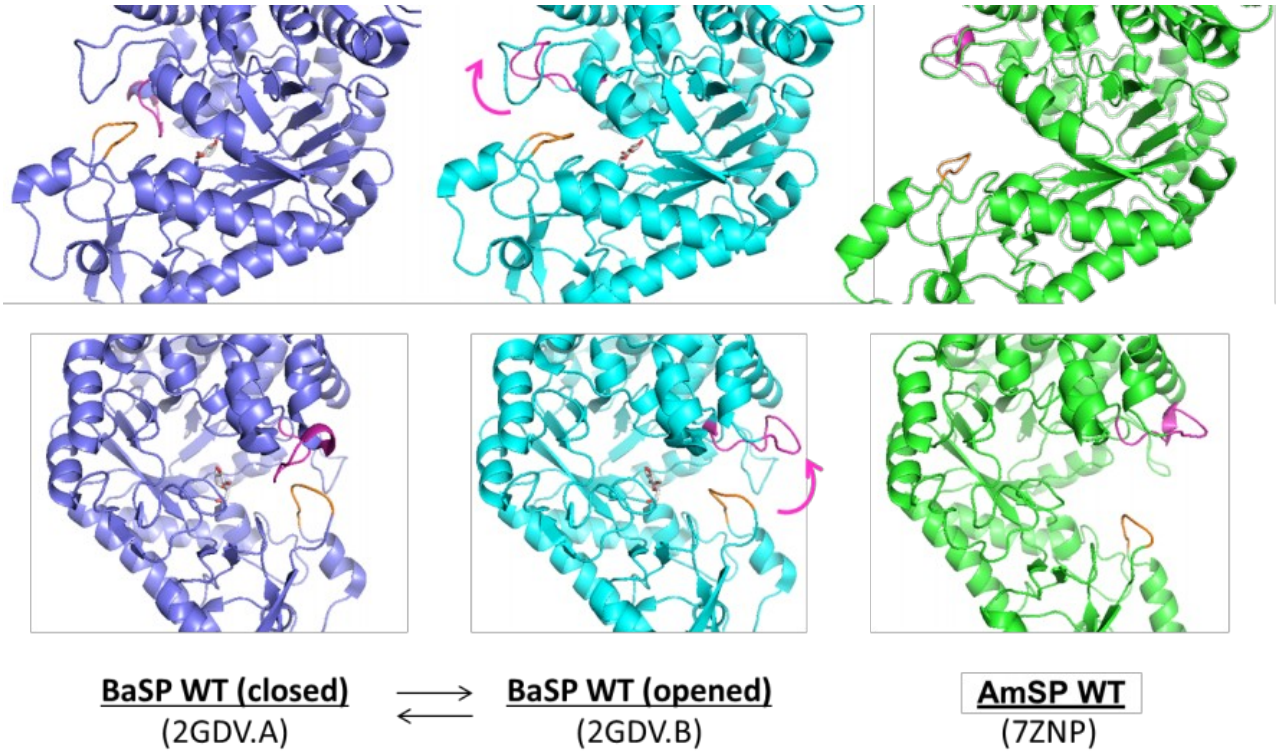

B.

*Ba*SP-WT	336	A	A	A	S	N	L	D*	L	Y*	Q*
*Am*SP-WT	344	A	A	A	S	N	L	D	L	Y	Q

C.

*Ba*SP-WT	132	Y*	R	P*	R*	P
*Am*SP-WT	138	F	R	P	R	P

Figure S1: Structural homology between *Ba*SP-WT and *Am*SP-WT. (A) Comparison of closed (purple) and opened (cyan) conformations of *Ba*SP and structure of *Am*SP WT (green). The functional loops are featured in magenta for loop A involved in sucrose binding and in orange for loop B involved with polyphenol binding. (B) Sequence comparison for loop A between BaSP and AmSP. (C) Sequence comparison for loop B between BaSP and AmSP.

*: these residues are involved in the binding of phosphate.

Table S1: Conserved residues and potential substrate interaction of *Am*SP. Potential substrate interaction and function of conserved residues were determined using structural homology between crystal structures of apoenzyme *Am*SP-WT (PDB: 7ZNP), apoenzyme *Ba*SP-WT (1R7A) and open conformation BaSP-WT (2GDV.B). Residue numbering of *Am*SP derived from crystal structure 7ZNP. Residue numbering of BaSP came from crystal structures 1R7A and 2GDV.B. Numbered OH-groups and C-atoms address to sucrose (apostrophe for fructosyl moiety), unless stated otherwise. [a]: residues from the -1 subsite, [b]: residues from the Loop A/+1 subsite, [c]: residues from the Loop B/+1 subsite. Approx.: Approximately the same position.

***Am*SP**	***Ba*SP**	**Conserved Conformation 1R7A/2GDV.B**	**Potential substrate interaction/remarks**	**Potential function**
Asp203 [a]	Asp192	Yes	Hydrogen bond with OH6	catalytic nucleophile
Glu243 [a]	Glu232	Yes	Hydrogen bond with OH1 and OH1’	general acid/base catalyst
Asp301 [a]	Asp290	Yes	Hydrogen bond with OH2	transition state stabiliser
Phe56 [a]	Phe53	Yes	hydrophobic/π interaction with C3-C4-C5; Cation-π interaction with oxocarbenium ion-like transition state	hydrophobic platform
Phe167 [a]	Phe156	Yes	hydrophobic/π interaction with C6 and C1’	hydrophobic platform
His91 [a]	His88	Approx.	Hydrogen bond with OH6	binding of glycosyl moiety
Arg201 [a]	Arg190	Yes	Hydrogen bond with OH2	binding of glycosyl moiety
His300 [a]	His289	Yes	Hydrogen bond with OH2 and OH3	binding of glycosyl moiety
Asp53 [a]	Asp50	Yes	Hydrogen bond with OH4	binding of glycosyl moiety
Arg407 [a]	Arg399	Yes	Hydrogen bond with OH3 and OH4	binding of glycosyl moiety
Gln171	Gln160	Approx.	Hydrogen bond with OH6	binding of glycosyl moiety
Ala204	Ala193	Yes	hydrophobic interaction with C6 and C1’	binding of glycosyl/fructosyl moiety
Leu351 [b]	Leu341	No	hydrophobic interaction with C6 and C6’	binding of glycosyl/fructosyl moiety
Tyr207	Tyr196	Approx.	hydrophobic/π interaction with C1’	involved in fructose binding
Asp350 [b]	Asp342	No/Approx.	Hydrogen bond with OH4’	involved in fructose binding
Gln353 [b]	Gln345	Yes	Hydrogen bond with O3’ and O6'	involved in fructose binding
Phe138 [c]	Tyr132	Approx.	at the entrance of active site; hydrophobic surroundings	Specificity for fructose
Pro140 [c]	Pro134	Approx.	in vicinity of C4-OH of fructose	involved in the binding of the fructose-bound phosphate group
Tyr207	Tyr196	Approx.	CE2-atom close to C1 of fructose	Specificity for fructose/phosphate
His245	His234	Yes	in vicinity of C3 and C3-OH of fructose	Specificity for fructose/phosphate
Arg141 [c]	Arg135	No/Approx.	Hydrogen bond with phosphate O; Specificity for fructose/phosphate	involved in phosphate binding
Leu351 [b]	Leu343	No/Yes	in between important residues Asp342 and Tyr344	Specificity for phosphate
Tyr352 [b]	Tyr344	No/Yes	Hydrogen bond with phosphate O	involved in phosphate binding
Ile244	Val233	Yes	next to the acid/base catalyst; side chain turned away from active site	unknown

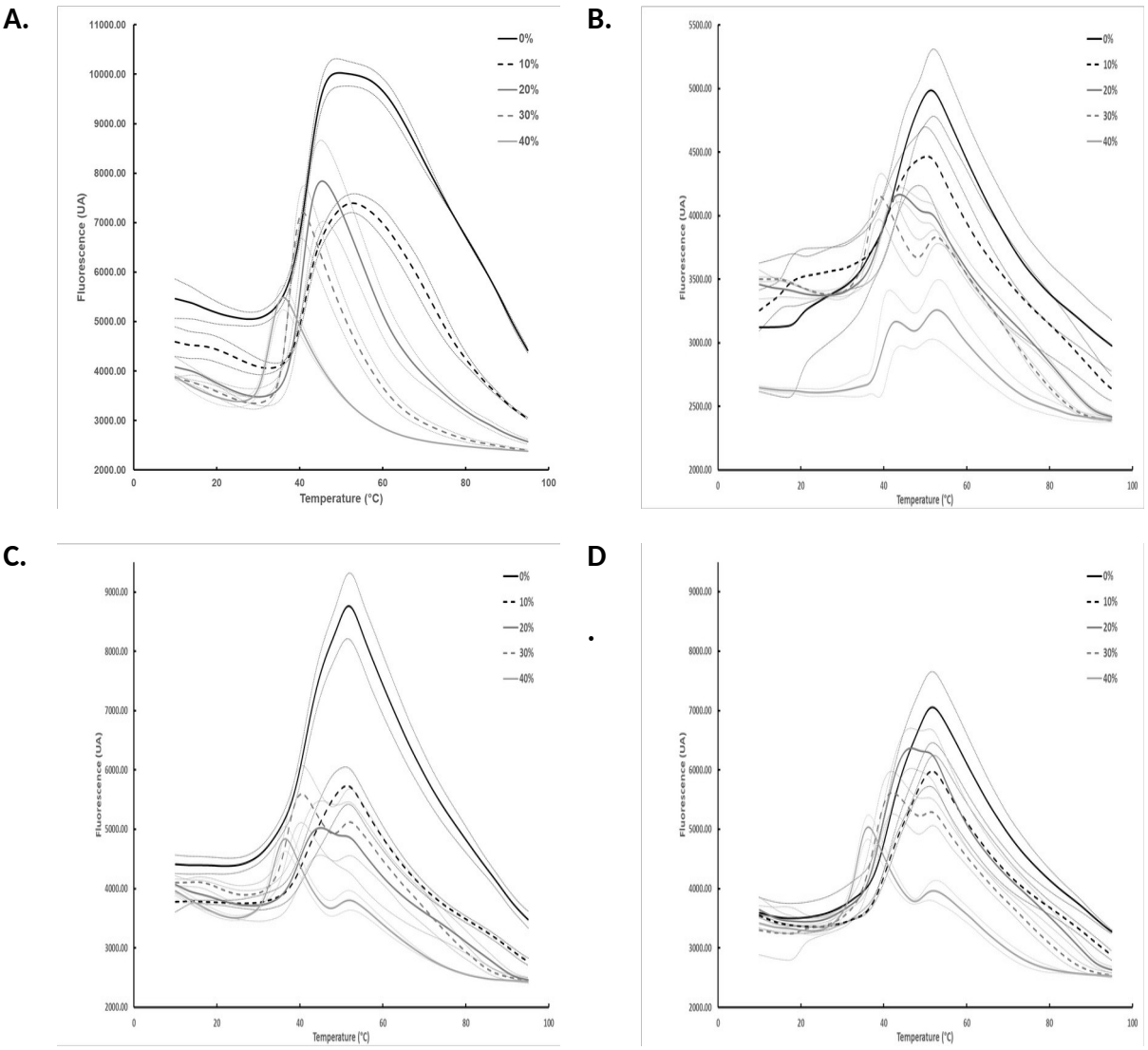

Figure S2: Melting curves of AmSP and its variants in MOPS-NaOH 50 mM pH 8.0 with DMSO from 0% to 40%. *(A) AmSP-WT, (B) AmSP-P140D, (C) AmSP-Q353F, (D) AmSP-P140D/Q353F*

Table S2: Melting temperature of *Am*SP and its variants. Values, given in °C, were obtained by calculating the first derivative -(dRFU)/dT of the melting curves.

	WT	P140D	Q353F	P140D/Q353F
H_2O	42.0 ± 0.0	42.8 ± 0.3	42.0 ± 0.9	42.2 ± 0.3
NPI-5	42.7 ± 0.3	42.5 ± 0.0	42.2 ± 0.3	41.5 ± 0.0
NPI-250	38.7 ± 0.3	38.2 ± 0.3	38.3 ± 0.3	37.3 ± 0.3
MOPS pH 7.0	44.8 ± 0.6	45.2 ± 0.3	44.0 ± 0.0	43.7 ± 0.3
pH 7.0 10%D	42.5 ± 0.0	42.2 ± 0.3	41.8 ± 0.3	42.3 ± 0.3
pH 7.0 20%D	39.5 ± 0.0	39.0 ± 0.0	39.2 ± 0.3	39.5 ± 0.0
pH 7.0 30%D	36.3 ± 1.0	36.3 ± 0.3	36.5 ± 0.5	36.7 ± 0.3
pH 7.0 40%D	31.3 ± 0.3	32.5 ± 0.0	32.7 ± 0.3	33.2 ± 0.3
MOPS pH 8.0	42.0 ± 0.0	43.0 ± 0.0	41.5 ± 0.0	41.2 ± 0.3
pH 8.0 10%D	41.3 ± 0.3	41.3 ± 0.4	41.5 ± 0.5	40.8 ± 1.0
pH 8.0 20%D	40.5 ± 0.0	39.3 ± 0.6	39.8 ± 0.3	39.5 ± 0.5
pH 8.0 30%D	37.5 ± 0.5	39.0 ± 0.7	37.0 ± 0.0	38.0 ± 0.5
pH 8.0 40%D	32.7 ± 0.3	39.5 ± 1.4	33.7 ± 0.3	33.7 ± 0.3
Citrate	45.5 ± 0.0	43.8 ± 0.4	43.5 ± 0.0	43.3 ± 0.3
HEPES	43.5 ± 0.3	44.0 ± 0.0	42.2 ± 0.6	42.2 ± 0.6
HEPES NaCl DTT	44.8 ± 0.6	45.0 ± 0.0	43.7 ± 0.8	44.3 ± 0.3

Determination of the apparent kinetic parameters

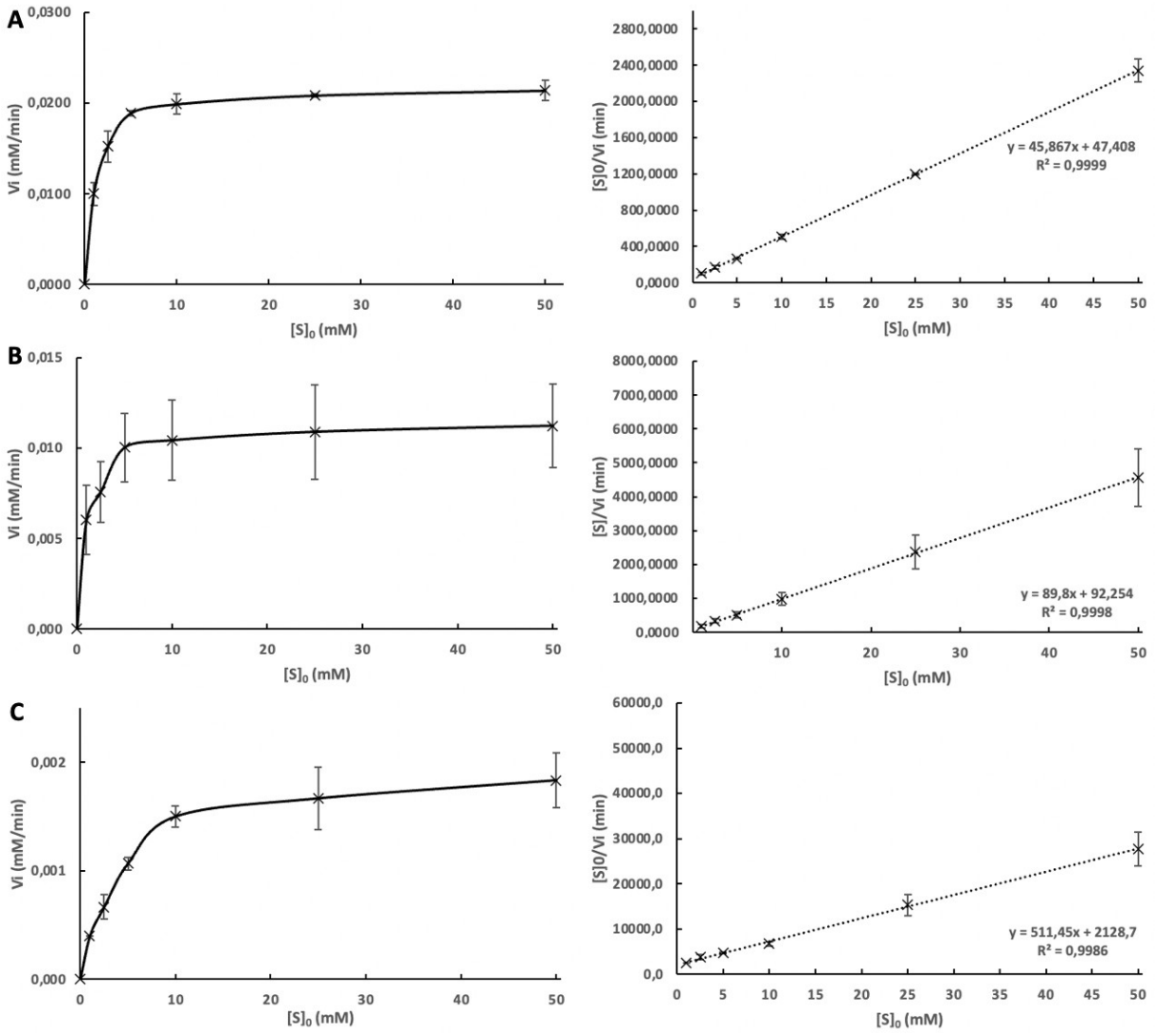

Figure S3: Kinetics and Hanes-Woolf plots of sucrose hydrolysis with DMSO 20% (v/v) by (A) *Am*dSP-WT, (B) *Am*dSP-P140D, (C) *Am*dSP-Q353F. Data were obtained by glucose titration (10 µM *Am*dSP-Q353F, 0.5-240 mM saccharose in MOPS-NaOH 50 mM pH 8.0 at 25°C).

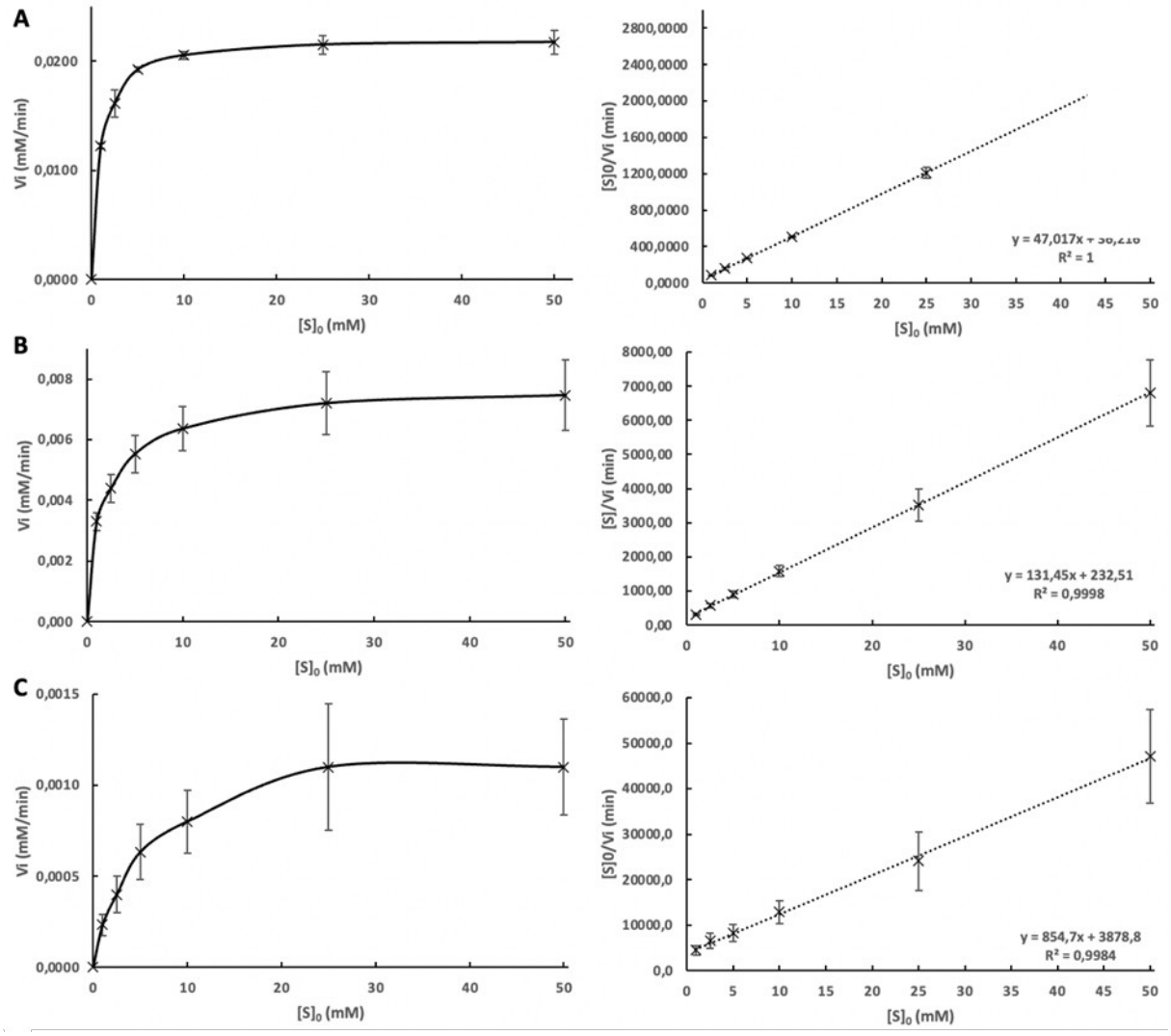

Figure S4: Kinetics and Hanes-Woolf plots of sucrose hydrolysis by (A) *Am*SP-WT, (B) *Am*SP-P140D, (C) *Am*SP-Q353F. Data were obtained by glucose titration (10 µM *Am*SP – Q353F , 0.5 – 240 mM saccharose in MOPS-NaOH 50 mM pH 8.0 at 25°C)

(+)-catechin transglycosylation studies

Synthesis yields

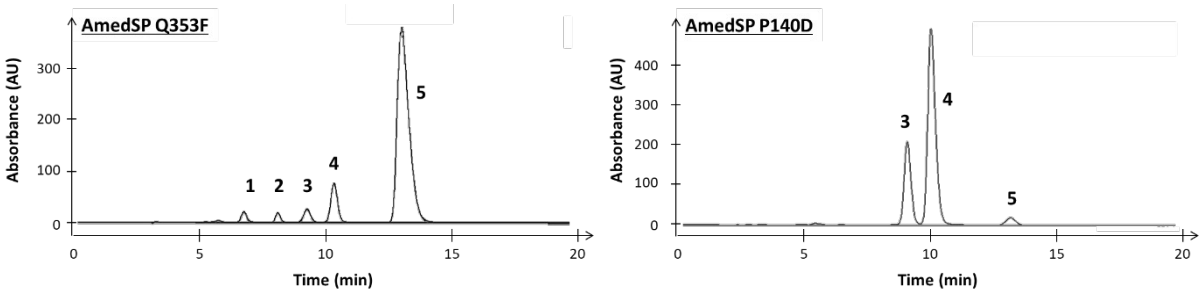

Figure S5: HPLC chromatogram of a 24 h reaction medium of (+)-catechin glucosylation by *Am*SP-WT variants. Peak 1: CAT-5, peak 2: CAT-3',5, peak 3: CAT-4', peak 4: (+)-catechin, peak 5: CAT-3'. Unassigned peaks correspond to impurities and degradation of (+)-catechin. (10 µM enzyme, 10 mM (+)-catechin, 80 mM sucrose, 20% DMSO (v/v) in MOPS 50 mM pH 8.0 at 25°C for 24 h). HPLC conditions: isocratic mode at 80% H_2O (v/v), 0.1% formic acid (v/v) and 20% MeOH (v/v), 0.1% formic acid (v/v).

^{1}H and ^{13}C NMR Spectral Data of CAT-4' in DMSO

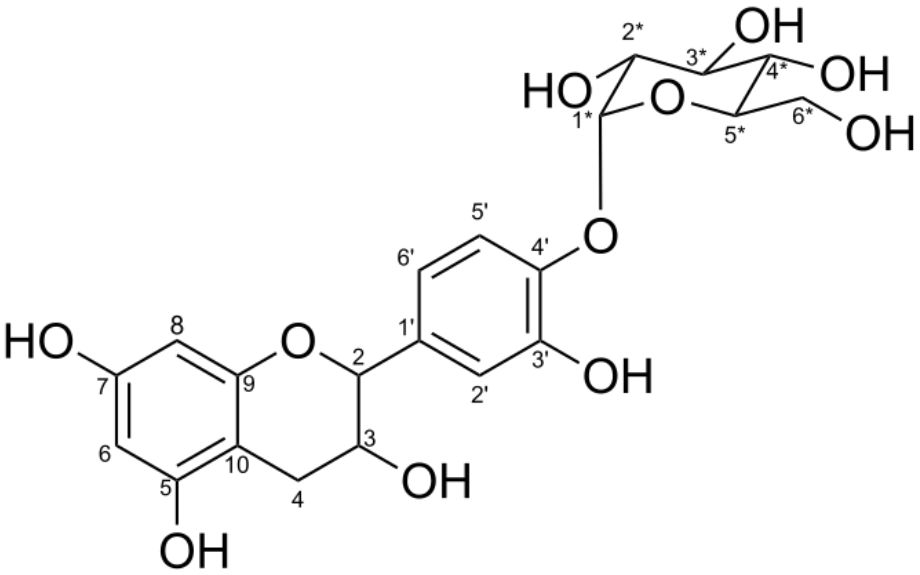

MS (ESI positive):

Ion Formula: $C_{21}H_{23}O_{11}$

m/z calculated: 451.1239

m/z experimental: 451.1240

error [ppm]: -0.2

^{1}H NMR (DMSO-d_6, δ) : 7.14 (d, $^{3}J_{5'-6'}$ = 8.3 Hz, 1H, $H_{5'}$), 6.80 (d, $^{3}J_{2'-6'}$ = 2.0 Hz, 1H, $H_{2'}$), 6.72 (dd, $^{3}J_{6'-2'}$ = 2.0 Hz, $^{3}J_{6'-5'}$ = 8.3 Hz, 1H, $H_{6'}$), 5.91 (d, $^{3}J_{6-8}$ = 2.2 Hz, 1H, H_6), 5.71 (d, $^{3}J_{8-6}$ = 2.2 Hz, 1H, H_8), 5.17 (d, $^{3}J_{1*-2*}$ = 3.6 Hz, 1H, H_{1*}), 4.55 (d, $^{3}J_{2-3}$ = 7.4 Hz, 1H, H_2), 3.85 (td, $^{3}J_{3-2}$ = 7.4 Hz, $^{3}J_{3-4a}$ = 5.3 Hz, $^{3}J_{3-4b}$ = 8.4 Hz, 1H, H_3), 3.71-3.65 (m, $^{3}J_{3*-2*}$ = 9.7 Hz, , 1H, H_{3*}), 3.65-3.62 (m, 1H, H_{6a*}), 3.55-3.49 (m, 1H, H_{5*}), 3.55-3.49 (m, 1H, H_{6b*}), 3.33 (dd, $^{3}J_{2*-1*}$ = 3.6 Hz, $^{3}J_{2*-3*}$ = 9.7 Hz, 1H, H_{2*}), 3.21-3.17 (m, 1H, H_{4*}), 2.65 (dd, $^{3}J_{4a-3}$ = 5.3 Hz, $^{2}J_{4a-4b}$ = 16.0 Hz, 1H, H_{4a}), 2.36 (dd, $^{3}J_{4b-3}$ = 8.4 Hz, $^{2}J_{4b-4a}$ = 16.3 Hz, 1H, H_{4b}).

^{13}C NMR (DMSO-d_6, δ) : 156.5 (C_7), 156.2 (C_5), 155.2 (C_{10}), 147.1 ($C_{4'}$), 144.7 ($C_{3'}$), 134.7 ($C_{1'}$), 118.2 ($C_{6'}$), 117.3 ($C_{5'}$), 114.8 ($C_{2'}$), 100.4 (C_{1*}), 99.0 (C_9), 95.2 (C_6), 93.8 (C_8), 80.7 (C_2), 73.8 (C_{5*}), 73.1 (C_{3*}), 72.0 (C_{2*}), 70.0 (C_{4*}), 66.3 (C_3), 60.7 (C_{6*}), 27.8 (C_4).

Table S4: Comparaison of ^{1}H and ^{13}C NMR Spectrum data of CAT-4' and (+)-catechin in DMSO. Multiplicity abbreviations for ^{1}H NMR: d = doublet, dd = doublet of doublets, td = pseudo triplet of doublets, m = multiplet. For characterization of CAT-3', CAT-5 and CAT-3',5 please see [10].

POSITION	CATECHIN ∂1H; J (HZ)	CAT-4' ∂1H; J (HZ)	CAT-4' ∂13C
1	X	X	X
2	4.48 (d 7.4)	4.55 (d 7.4)	80.67
3	3.82 (td 8.1, 7.4, 5.2)	3.85 (td 8.4, 7.4, 5.33)	66.26
4	2.67 (dd 16.1, 5.2) 2.35 (dd 16.0, 8.1)	2.65 (dd 16.0, 5.3) 2.36 (dd 16.3, 8.4)	27.84
5	X	X	156.21
6	5.89 (d 2.2)	5.91 (d 2.2)	95.22
7	X	X	156.51
8	5.69 (d 2.2)	5.71 (d 2.2)	93.78
9	X	X	98.95
10	X	X	155.17
1'	X	X	134.68
2'	*6.73 (d 1.9)*	*6.80 (d 2.0)*	114.79
3'	X	X	144.71
4'	X	X	147.06
5'	*6.69 (d 8.1)*	*7.14 (d 8.3)*	117.26
6'	*6.60 (dd 8.1, 1.9)*	*6.72 (dd 8.3, 2.0)*	118.16
1*	X	5.17 (d 3.6)	100.40
2*	X	3.33 (dd 9.7, 3.6)	72.02
3*	X	3.71-3.65 (m)	73.06
4*	X	3.21-3.17 (m)	69.96
5*	X	3.59-3.55 (m)	73.75
6*	X	3.65-3.62 (m) 3.55-3.49 (m)	60.73

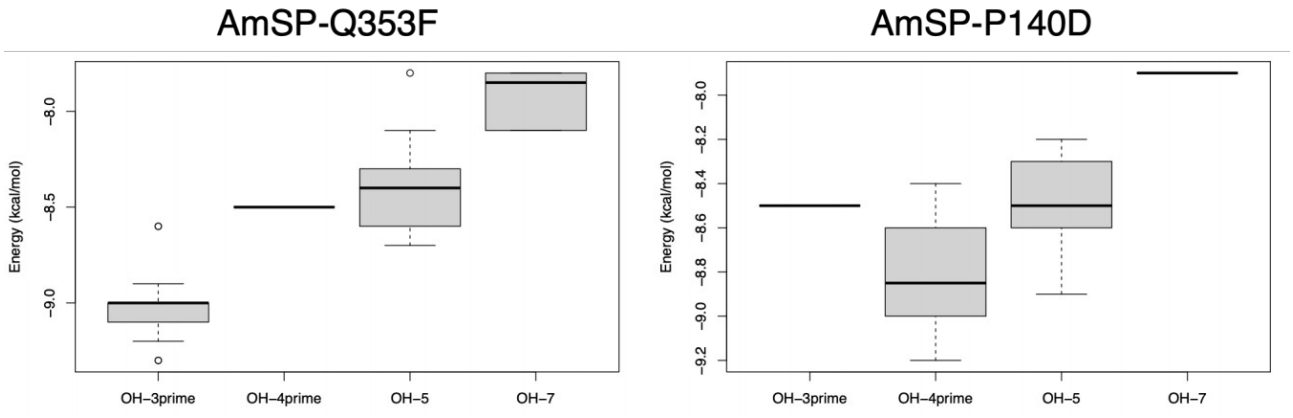

Figure S6: Statistical analysis of the binding energies of productive poses for glucosylation of (+) catechin in OH-3', OH-4', OH-5 and OH-7 positions with Q353F and P140D. Molecular docking poses were filtered by considering those with an oxygen of (+)-catechin within 3 Å of the C1 atom of the glucosyl moiety as productive (see sections 2.4, 2.5 and 3.4 in main text for additional details).

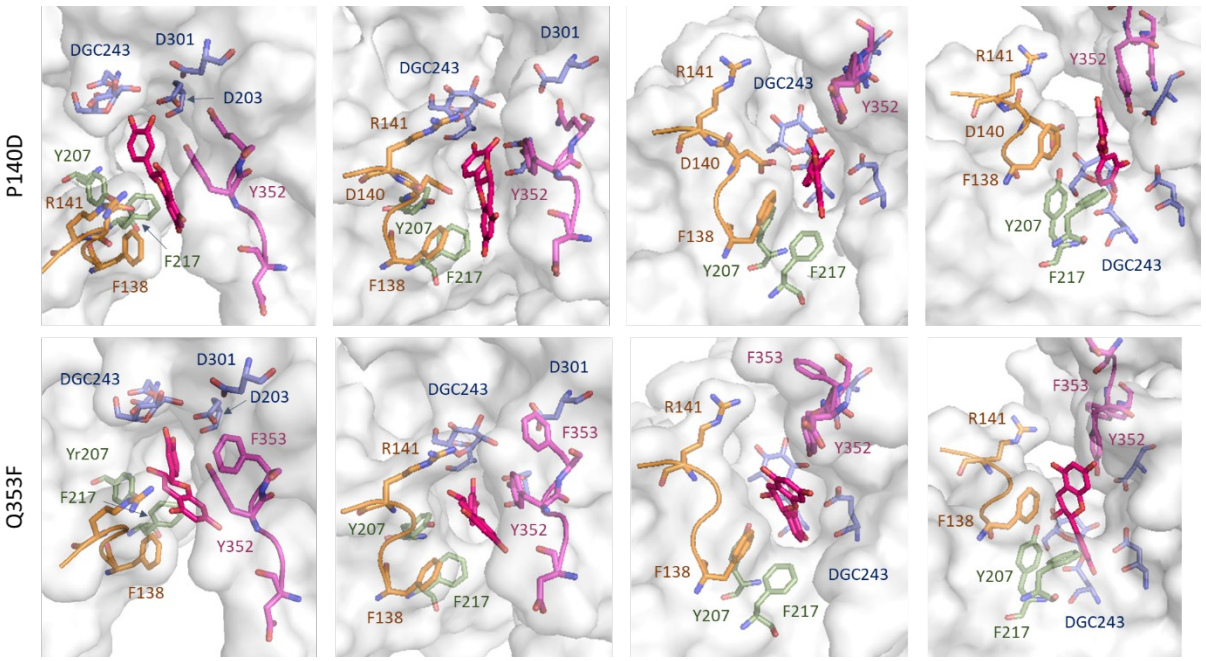

Figure S7: Different views of the position of the best productive poses of (+)-catechin in the active site of *Am*SP-P140D and *Am*SP-Q353F. In magenta: Loop A with in sticks Y352/F350/Q(F)353 residues; orange: Loop B with in sticks R141/F138 and D140 for *Am*SP-P140D; blue: residues of the catalytic triad with in sticks D203/D301/DGC243; green: aromatic residues involved in steric clash with in sticks Y207 and F217; and pink: (+)-catechin.